Simulation	Method	AMI	NMI	ARI	Precision	Recall	F_1
Dataset I-1	Gaussian-HMM	0.7863	0.8216	0.5941	0.8206	0.5569	0.6629
Dataset I-1	GMM	0.7562	0.7985	0.6340	**0.8903**	0.5679	0.6932
Dataset I-1	Clustering	0.6471	0.6926	0.4752	0.7539	0.4412	0.5558
Dataset I-1	Phylo-HMM-BM	0.8190	0.8494	0.7801	0.8496	0.8122	0.8226
Dataset I-1	Phylo-HMM-OU ($\lambda_0 = 0$)	0.7966	0.8183	0.6088	0.7973	0.5918	0.6786
Dataset I-1	Phylo-HMM-OU ($\lambda_0 = 4.0$)	**0.8309**	**0.8733**	**0.8405**	0.8568	**0.8986**	**0.8728**
Dataset I-2	Gaussian-HMM	0.5342	0.6901	0.2931	0.9666	0.2948	0.4519
Dataset I-2	GMM	0.3446	0.4508	0.1884	0.8114	0.2335	0.3625
Dataset I-2	Clustering	0.2692	0.3599	0.1157	0.7173	0.1768	0.2837
Dataset I-2	Phylo-HMM-BM	0.5208	0.6621	0.3150	0.9531	0.3218	0.4810
Dataset I-2	Phylo-HMM-OU ($\lambda_0 = 0$)	0.5315	0.6782	0.3149	0.9602	0.3191	0.4790
Dataset I-2	Phylo-HMM-OU ($\lambda_0 = 4.0$)	**0.7691**	**0.8229**	**0.7638**	**0.9811**	**0.7718**	**0.8565**
Dataset I-3	Gaussian-HMM	0.7323	0.7912	0.4919	0.8314	0.4476	0.5819
Dataset I-3	GMM	0.5536	0.6200	0.3354	0.7442	0.3057	0.4334
Dataset I-3	Clustering	0.4973	0.5561	0.2798	0.6580	0.2741	0.3870
Dataset I-3	Phylo-HMM-BM	0.6752	0.7277	0.4282	0.7646	0.4045	0.5283
Dataset I-3	Phylo-HMM-OU ($\lambda_0 = 0$)	0.7146	0.7698	0.4741	0.8088	0.4372	0.5674
Dataset I-3	Phylo-HMM-OU ($\lambda_0 = 4.0$)	**0.8309**	**0.8733**	**0.8405**	**0.8568**	**0.8986**	**0.8728**
Dataset I-4	Gaussian-HMM	0.6965	0.7967	0.4824	0.9585	0.4482	0.6095
Dataset I-4	GMM	0.7185	0.8106	0.5241	0.9737	0.4849	0.6457
Dataset I-4	Clustering	0.5812	0.6810	0.3535	0.8928	0.3395	0.4911
Dataset I-4	Phylo-HMM-BM	0.8151	0.8644	0.7342	**0.9756**	0.7112	0.8174
Dataset I-4	Phylo-HMM-OU ($\lambda_0 = 0$)	0.7946	0.8544	0.6846	0.9736	0.6589	0.7776
Dataset I-4	Phylo-HMM-OU ($\lambda_0 = 4.0$)	**0.8396**	**0.8607**	**0.8146**	0.9687	**0.8071**	**0.8792**
Dataset I-5	Gaussian-HMM	0.7688	0.8331	0.5644	0.9091	0.4908	0.6374
Dataset I-5	GMM	0.6398	0.6949	0.5065	0.8366	0.4552	0.5893
Dataset I-5	Clustering	0.5298	0.5906	0.3494	0.7227	0.3218	0.4453
Dataset I-5	Phylo-HMM-BM	0.7654	0.8243	0.5594	0.8908	0.4929	0.6346
Dataset I-5	Phylo-HMM-OU ($\lambda_0 = 0$)	0.7738	0.8370	0.5809	0.9180	0.5057	0.6521
Dataset I-5	Phylo-HMM-OU ($\lambda_0 = 4.0$)	**0.8798**	**0.9187**	**0.9594**	**0.9524**	**0.9867**	**0.9692**
Dataset I-6	Gaussian-HMM	0.8736	**0.9141**	0.7466	**0.9642**	0.6635	0.7861
Dataset I-6	GMM	0.7810	0.8157	0.6810	0.8884	0.6215	0.7312
Dataset I-6	Clustering	0.6409	0.6785	0.5101	0.7457	0.4791	0.5833
Dataset I-6	Phylo-HMM-BM	0.8554	0.8772	0.7534	0.9052	0.7133	0.7932
Dataset I-6	Phylo-HMM-OU ($\lambda_0 = 0$)	0.8538	0.8891	0.7216	0.9325	0.6490	0.7652
Dataset I-6	Phylo-HMM-OU ($\lambda_0 = 4.0$)	**0.8906**	0.8958	**0.8390**	0.9224	**0.8200**	**0.8678**

Table S1: Performance evaluation of Gaussian-HMM, GMM (Gaussian Mixture Model), K-means Clustering, Phylo-HMGP-BM, Phylo-HMGP-OU ($\lambda_0 = 0$), and Phylo-HMGP-OU ($\lambda_0 = 4.0$) on six simulated datasets in Simulation Study I with respect to AMI (Adjusted Mutual Information), NMI (Normalized Mutual Information), ARI (Adjusted Rand Index), Precision, Recall, and F_1 score. Related to Figure 2. Each method is repeated 10 times with different initializations on each simulation dataset. The average performance from the 10 repeated runs of each method is presented. The best performance of the compared methods is in bold font.

Simulation	Method	AMI	NMI	ARI	Precision	Recall	F_1
Dataset II-1	Gaussian-HMM	0.8314	0.8765	0.6693	**0.9244**	0.5965	0.7251
Dataset II-1	GMM	0.7399	0.7823	0.6138	0.8800	0.5511	0.6776
Dataset II-1	Clustering	0.6144	0.6623	0.4509	0.7579	0.4124	0.5341
Dataset II-1	Phylo-HMM-BM	0.8511	**0.8796**	**0.7786**	0.8785	**0.7842**	**0.8205**
Dataset II-1	Phylo-HMM-OU	**0.8534**	0.8706	0.7385	0.8319	0.7591	0.7906
Dataset II-2	Gaussian-HMM	0.5328	0.6863	0.2957	0.9550	0.3099	0.4680
Dataset II-2	GMM	0.3421	0.4477	0.1893	0.8206	0.2416	0.3733
Dataset II-2	Clustering	0.2590	0.3481	0.1119	0.7278	0.1780	0.2860
Dataset II-2	Phylo-HMM-BM	0.5343	0.6877	0.2944	0.9550	0.3085	0.4663
Dataset II-2	Phylo-HMM-OU	**0.6901**	**0.7833**	**0.5883**	**0.9736**	**0.6033**	**0.7353**
Dataset II-3	Gaussian-HMM	0.7754	0.8307	0.5236	**0.8469**	0.4700	0.6045
Dataset II-3	GMM	0.5641	0.6248	0.3463	0.7225	0.3176	0.4412
Dataset II-3	Clustering	0.5098	0.5606	0.2991	0.6385	0.2963	0.4048
Dataset II-3	Phylo-HMM-BM	0.7239	0.7727	0.4652	0.7793	0.4338	0.5561
Dataset II-3	Phylo-HMM-OU	**0.8159**	**0.8952**	**0.8797**	**0.8469**	**0.9848**	**0.9105**
Dataset II-4	Gaussian-HMM	0.6585	0.7623	0.4139	0.9318	0.3898	0.5497
Dataset II-4	GMM	0.7451	0.8262	0.5859	**0.9778**	0.5486	0.7027
Dataset II-4	Clustering	0.5411	0.6463	0.2933	0.8678	0.2868	0.4307
Dataset II-4	Phylo-HMM-BM	0.7857	0.8411	0.6904	0.9543	0.6812	0.7775
Dataset II-4	Phylo-HMM-OU	**0.8092**	**0.8556**	**0.7135**	0.9583	**0.7045**	**0.7981**
Dataset II-5	Gaussian-HMM	0.7932	0.8529	0.5842	0.9078	0.5125	0.6551
Dataset II-5	GMM	0.6640	0.7155	0.5399	0.8595	0.4827	0.6173
Dataset II-5	Clustering	0.5317	0.5894	0.3375	0.7028	0.3142	0.4343
Dataset II-5	Phylo-HMM-BM	0.7999	0.8595	0.5891	0.9223	0.5139	0.6573
Dataset II-5	Phylo-HMM-OU	**0.9162**	**0.9454**	**0.9504**	**0.9555**	**0.9694**	**0.9622**
Dataset II-6	Gaussian-HMM	0.8600	0.8969	0.7162	**0.9411**	0.6396	0.7613
Dataset II-6	GMM	0.7742	0.8118	0.6665	0.8887	0.6050	0.7197
Dataset II-6	Clustering	0.6319	0.6733	0.5036	0.7554	0.4689	0.5784
Dataset II-6	Phylo-HMM-BM	0.8371	0.8612	0.7241	0.8788	0.6944	0.7701
Dataset II-6	Phylo-HMM-OU	**0.9117**	**0.9150**	**0.8632**	0.9314	**0.8506**	**0.8888**

Table S2: Performance evaluation of Gaussian-HMM, GMM, K-means Clustering, Phylo-HMGP-BM, and Phylo-HMGP-OU ($\lambda_0 = 4.0$) on six simulated datasets in Simulation Study II with respect to AMI, NMI, ARI, Precision, Recall, and F_1 score. Related to Figure 2. Each method is repeated 10 times with different initializations on each simulation dataset. The average performance from the 10 repeated runs of each method is presented. The best performance of the compared methods is in bold font.

Conserved RT early	GO term/Pathway	Count	Fold enrichment	p-value
Constitutive RT early	intracellular transport	431	1.2	6.4e-06
	amide biosynthetic process	214	1.3	1.5e-05
	posttranscriptional regulation of gene expression	149	1.4	2.0e-05
	cellular amide metabolic process	277	1.2	2.0e-05
	peptide biosynthetic process	195	1.3	2.4e-05
	peptide metabolic process	231	1.3	2.5e-05
	mRNA metabolic process	193	1.2	5.8e-05
	translation	187	1.3	5.9e-05
	microtubule-based process	179	1.3	1.0e-04
	clathrin-mediated endocytosis	22	2.1	3.0e-04
	regulation of vascular permeability	18	2.3	3.9e-04
	mitochondrion organization	183	1.2	7.2e-04
Non-constitutive RT early	immune response	540	1.3	7.9e-013
	regulation of immune response	327	1.3	2.7e-010
	defense response	520	1.2	5.5e-08
	symbiosis, encompassing mutualism through parasitism	376	1.2	5.7e-08
	interspecies interaction between organisms	376	1.2	5.7e-08
	viral process	362	1.2	1.2e-07
	multi-organism cellular process	364	1.2	1.7e-07
	immune effector process	257	1.3	2.6e-07
	immune response-activating signal transduction	176	1.4	7.9e-07
	activation of immune response	192	1.3	1.1e-06
	immune response-regulating signaling pathway	186	1.3	1.2e-06
	regulation of immune system process	465	1.2	2.5e-06

Table S3: Gene ontology (GO) terms or pathways that show significant correlation with regions that are both constitutive RT early and conserved RT early, and regions that are conserved RT early but not constitutive RT early. Related to Figure 3. We used DAVID to perform the gene ontology analysis. The column Count represents the number of genes found to be associated with the corresponding GO term/pathway in the queried regions. The conserved early RT regions are based on state prediction by Phylo-HMGP. We observed that genes enriched in the regions that are both constitutive early and conserved early are mainly involved in basic biological functions and processes that are shared between different cell types. Genes associated with the regions that are not constitutive early but conserved early are involved in the cell type specific functions of the lymphoblastoid cells, such as the immune response functions.

Predicted state	GO term/Pathway	Count	Fold enrichment	p-value
State 9	sensory perception of smell	16	8.5	1.9e-09
	detection of chemical stimulus	17	6.6	6.3e-09
	detection of stimulus involved in sensory perception	17	6.4	9.2e-09
	olfactory transduction	16	6.0	4.1e-08
	sensory perception	21	2.9	3.6e-05
	neurological system process	23	2.2	8.2e-04
State 10	regulation of nucleic acid-templated transcription	95	1.5	1.4e-05
	regulation of RNA biosynthetic process	95	1.5	1.9e-05
	regulation of nucleobase-containing compound metabolic process	101	1.4	1.4e-04
	aromatic compound biosynthetic process	107	1.4	1.5e-04
	heterocycle biosynthetic process	106	1.4	2.1e-04
	regulation of nitrogen compound metabolic process	104	1.3	5.8e-04
	cellular macromolecule biosynthetic process	114	1.3	1.1e-03
State 11	G-protein coupled purinergic nucleotide receptor signaling pathway	4	33.2	2.0e-04
	cellular response to organic substance	32	1.8	1.6e-03
	insulin secretion	6	5.0	6.7e-03
	response to endogenous stimulus	23	1.8	9.6e-03
State 14	endocardial cushion morphogenesis	7	15.6	4.4e-06
	cartilage development	13	4.9	1.4e-05
	endocardial cushion development	7	11.6	2.7e-05
	connective tissue development	14	4.1	4.1e-05
	pattern specification process	18	2.8	2.1e-04
	organ morphogenesis	29	2.0	5.1e-04
	enzyme linked receptor protein signaling pathway	27	2.0	1.1e-03
	circulatory system development	27	2.0	1.3e-03
	cardiovascular system development	27	2.0	1.3e-03
State 16	cell adhesion	27	2.2	1.4e-04
	regulation of nervous system development	15	2.6	1.5e-03
	regulation of neurogenesis	13	2.6	4.3e-03
	regulation of cellular component organization	29	1.7	4.5e-03
	neuron projection morphogenesis	11	2.8	6.1e-03
	neuron differentiation	18	2.0	8.3e-03
State 18	regulation of locomotion	32	2.6	1.4e-06
	regulation of cell motility	31	2.7	1.6e-06
	regulation of cell migration	29	2.7	3.5e-06
	regulation of cell differentiation	45	1.9	4.0e-05
	epithelium development	33	1.9	3.4e-04
	cell proliferation	43	1.5	6.6e-03
	regulation of anatomical structure morphogenesis	28	1.7	7.8e-03
	movement of cell or subcellular component	42	1.5	8.3e-03

Table S4: Example gene ontology (GO) terms or pathways that show significant correlation with lineage-specific RT states (State 9: human-chimpanzee specific early RT state; State 10: human-chimpanzee specific late RT state; State 11: human-chimpanzee-orangutan specific early RT state; State 14: orangutan specific late RT state; State 16: gibbon specific late RT state; State 18: green monkey specific late RT state). Related to Figure 4. We use DAVID to perform the gene ontology analysis.

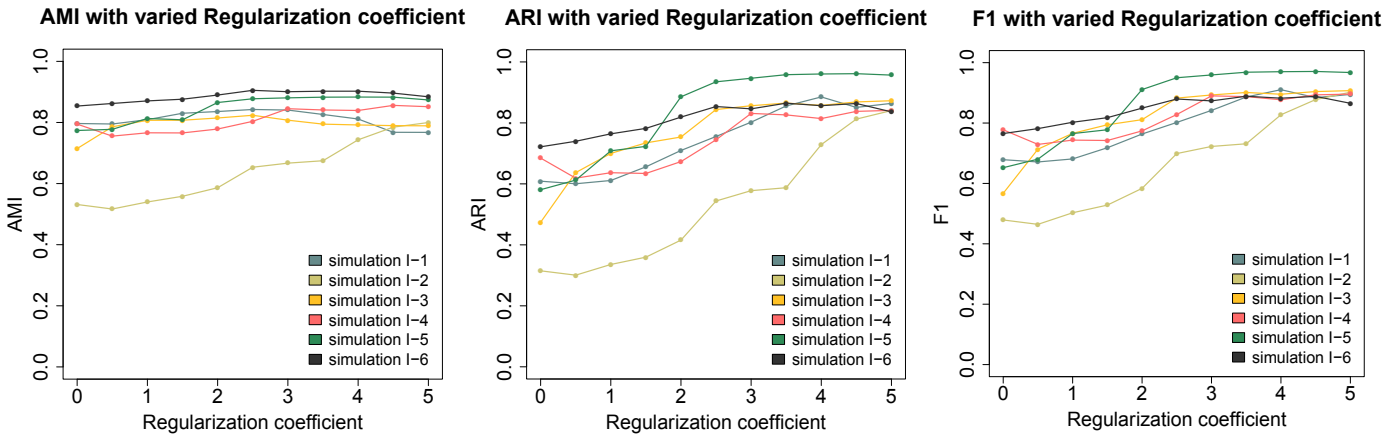

Figure S1: Performance evaluation on AMI, ARI, and F_1 score in Simulation Study I with respect to varied l_2-norm regularization coefficient λ_0. Related to Figure 2.

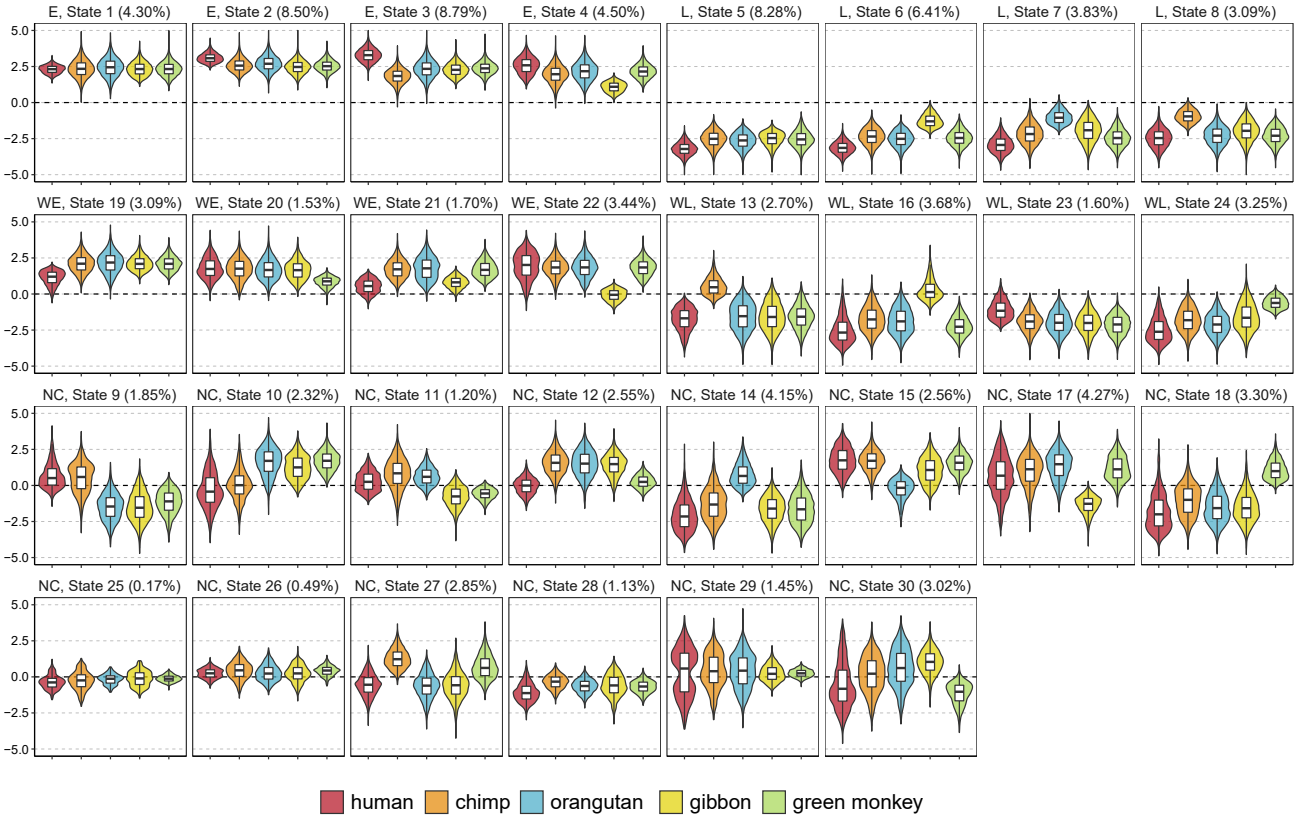

Figure S2: Different patterns of replication timing (RT) across five primate species predicted by Phylo-HMGP-OU for 30 states. Related to Figure 3. The y-axis represents the RT signal value. Box plots of the RT signal distributions of the five primate species in each predicted state are shown. The percentage of the number of regions in each predicted state and the RT group label are also shown in the title of each plot.

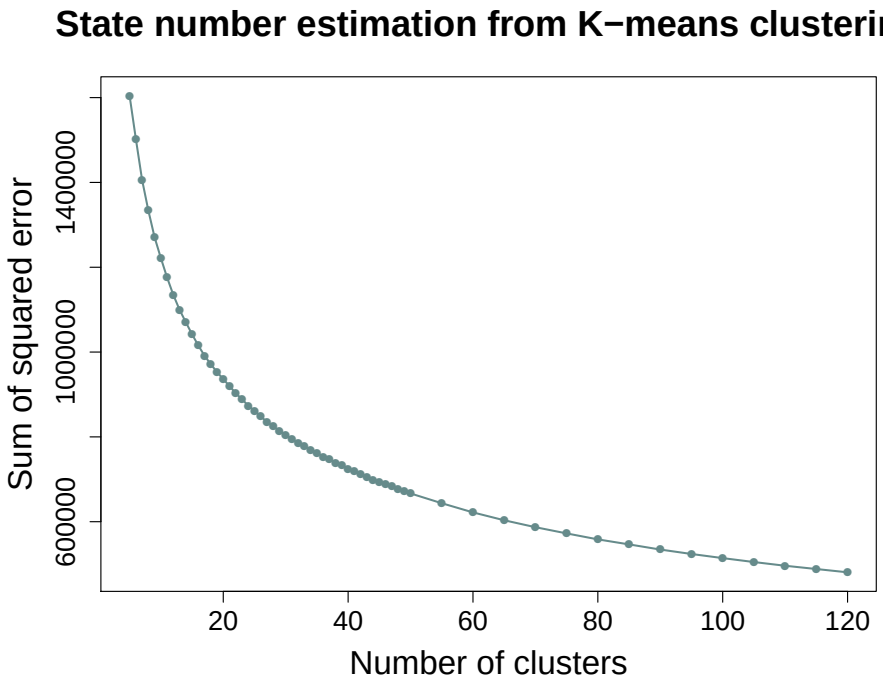

Figure S3: The change of Sum of Squared Error (SSE) with respect to an increased cluster number in K-means clustering on RT data. Related to Figure 3. The state number was estimated to be between 20 and 40 based on the results from K-means clustering.

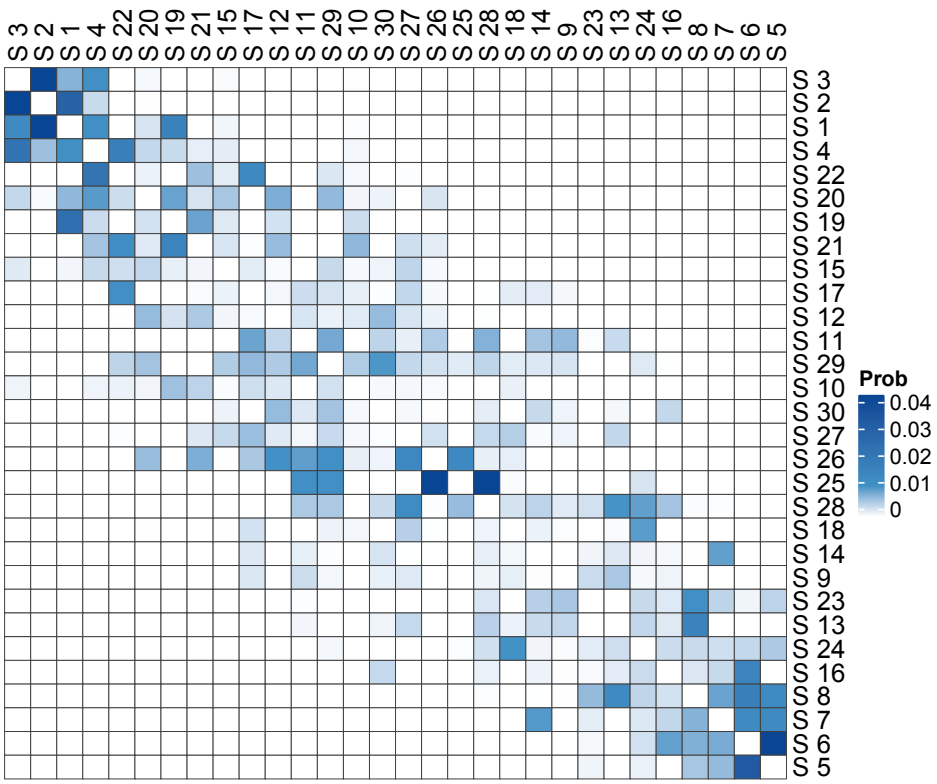

Figure S4: Transition probability matrix of the 30 states estimated by Phylo-HMGP-OU. Related to Figure 3. The self-transition probability is not shown (set to be blank) to illustrate the probabilities of transitions to other states more significantly.

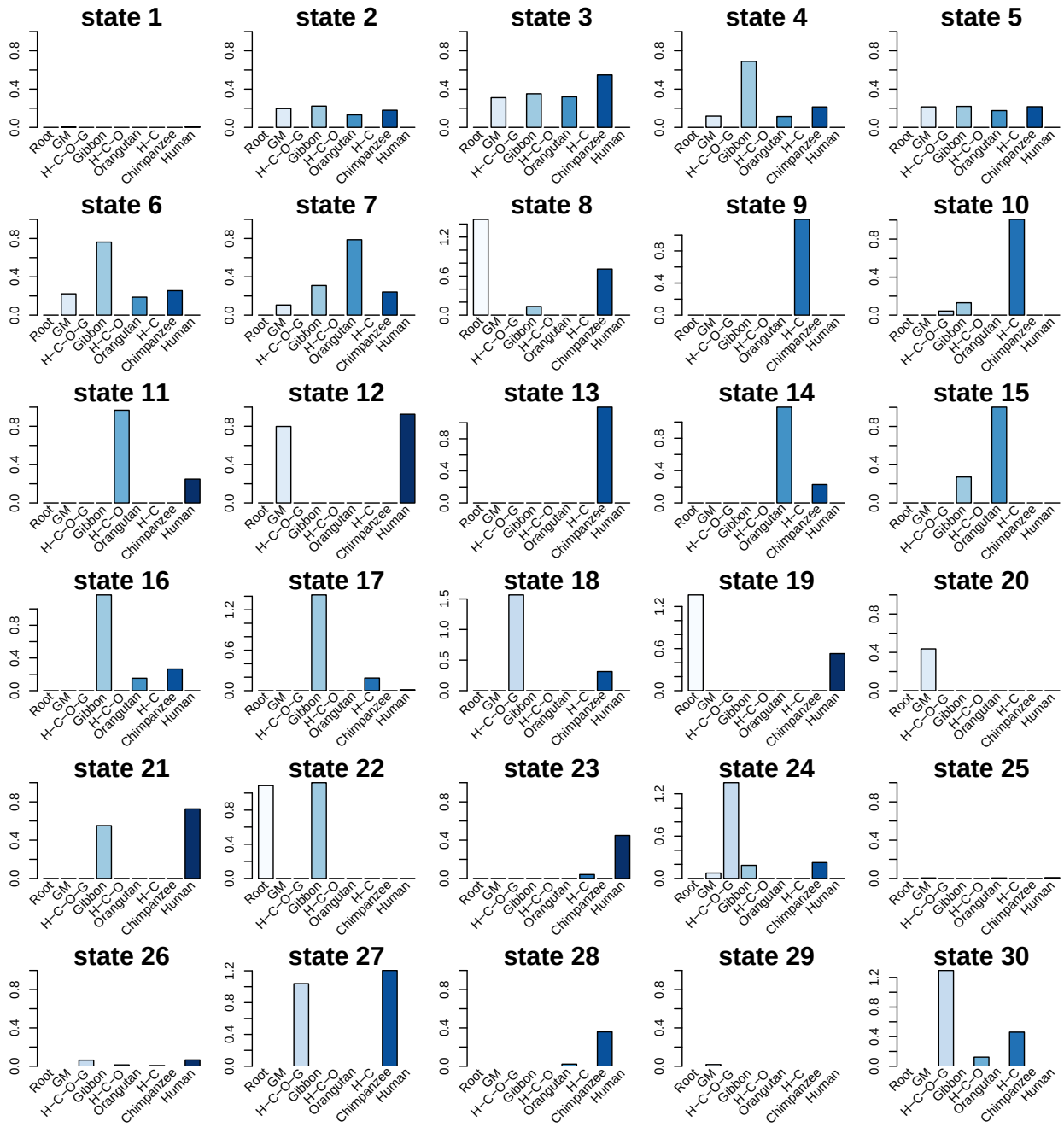

Figure S5: Estimated selection strength along each branch of the phylogenetic tree in the 30 states predicted by Phylo-HMGP-OU. Related to Figure 3. 'GM' stands for Green Monkey. Each column corresponds to the branch connecting the nearest ancestor of the species specified by the species name to the species. Root stands for the branch connecting the remote root node ancestor with the nearest common ancestor of green monkey and human. H-C-O-G, H-C-O, and H-C represent the branches leading to the clade of human, chimpanzee, orangutan, and gibbon, the clade of human, chimpanzee, and orangutan, and the clade of human and chimpanzee, respectively.

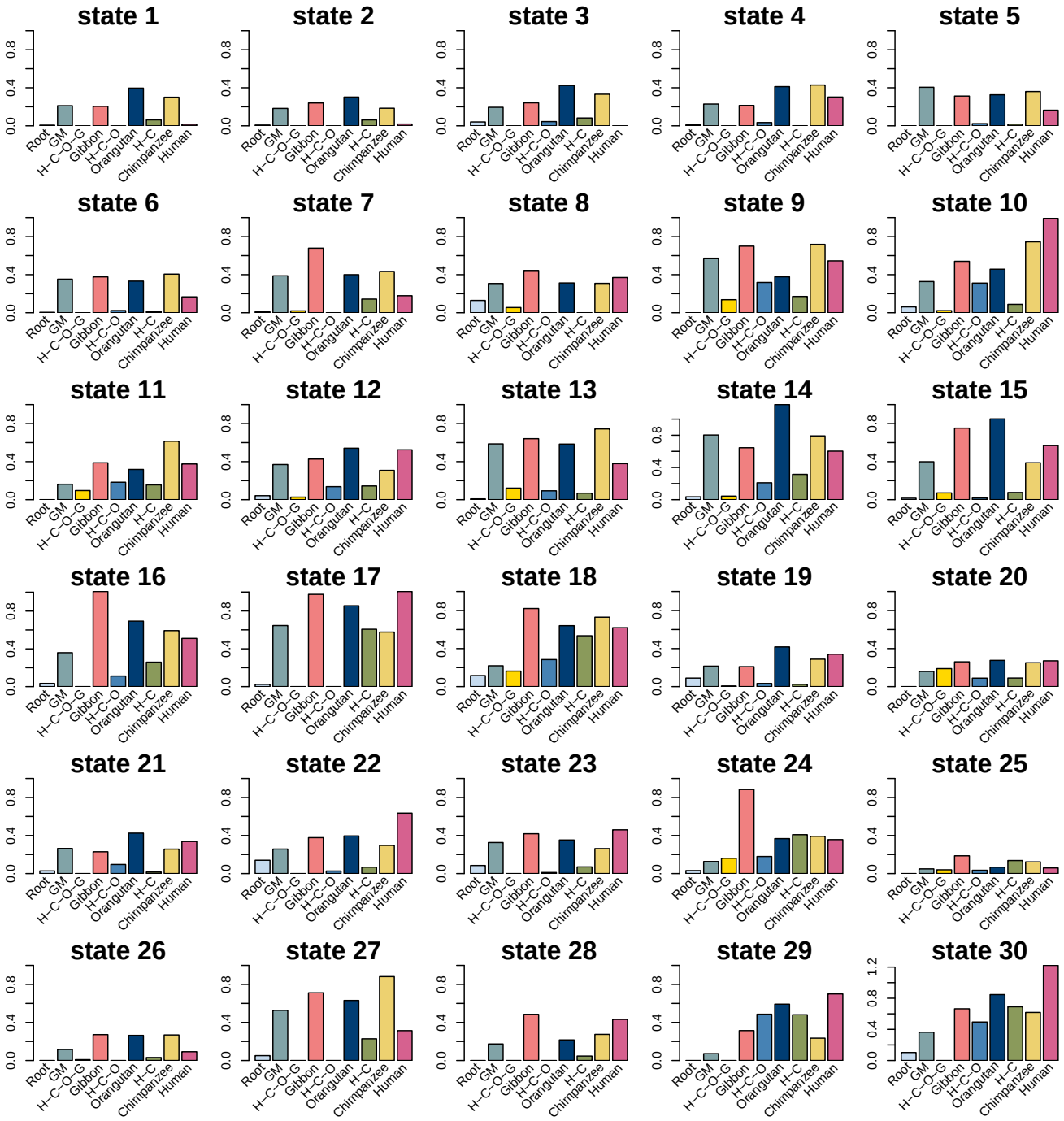

Figure S6: Estimated Brownian motion intensity along each branch of the phylogenetic tree in the 30 states predicted by Phylo-HMGP-OU. Related to Figure 3. 'GM' stands for Green Monkey. Each column corresponds to the branch connecting the nearest ancestor of the species specified by the species name to the species. Root stands for the branch connecting the remote root node ancestor with the nearest common ancestor of green monkey and human. H-C-O-G, H-C-O, and H-C represent the branches leading to the clade of human, chimpanzee, orangutan, and gibbon, the clade of human, chimpanzee, and orangutan, and the clade of human and chimpanzee, respectively.

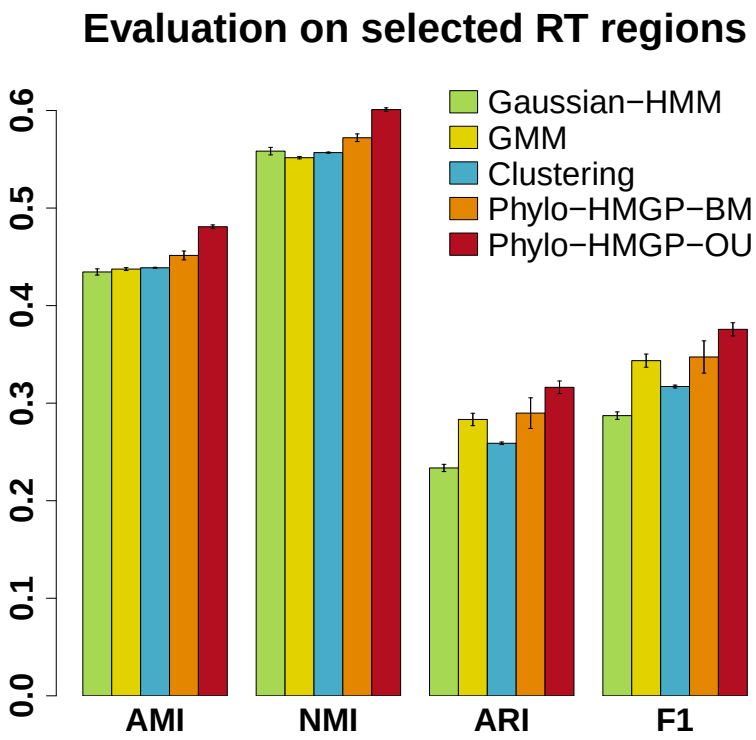

Figure S7: Evaluation of Gaussian-HMM, GMM, K-means Clustering, Phylo-HMGP-BM, and Phylo-HMGP-OU on the replication timing dataset in terms of AMI, NMI, ARI and F_1 score in the genomic regions of 12 different states (including 10 lineage-specific states and two conserved states) identified from comparison of discretized single-species observations. Related to Figure 3. The standard error of the results of 10 repeated runs for each method is shown as the error bar.

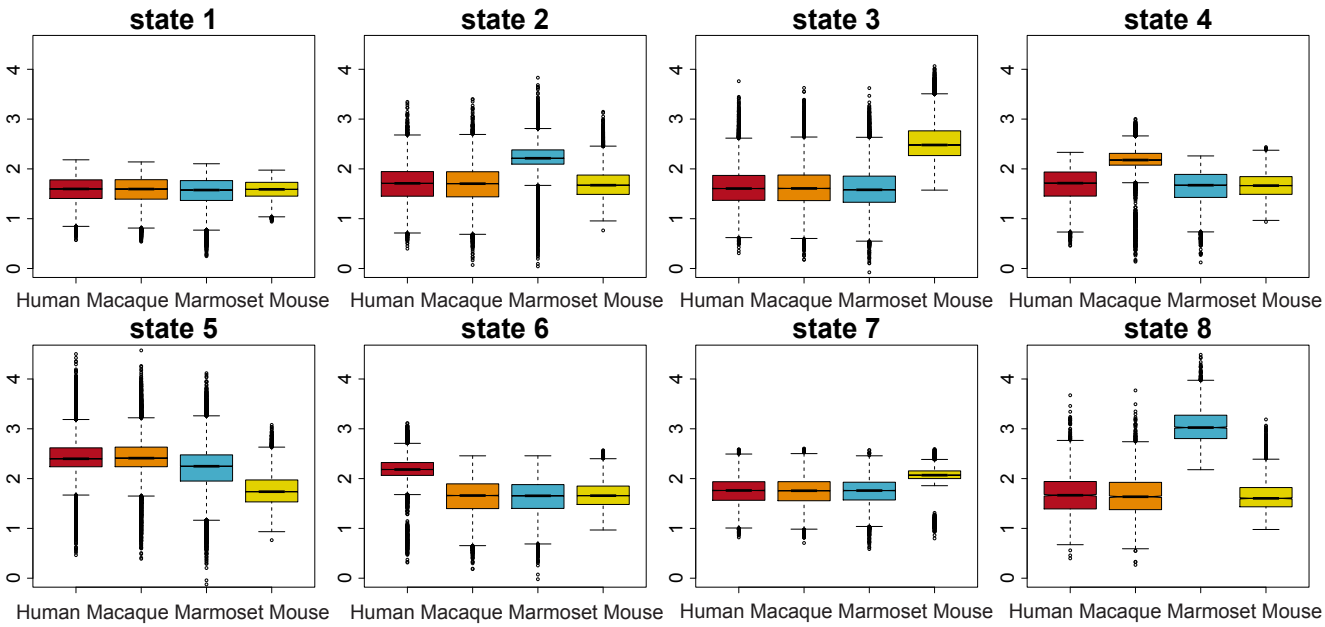

Figure S8: Different patterns of CRM (*cis*-regulatory module) score across four mammalian species (human, macaque, marmoset, and mouse) predicted by Phylo-HMGP-OU. Related to Figure 1. Box plots of the top 8 states with the most number of genomic regions are shown. The y-axis represents the logarithm of the CRM score.

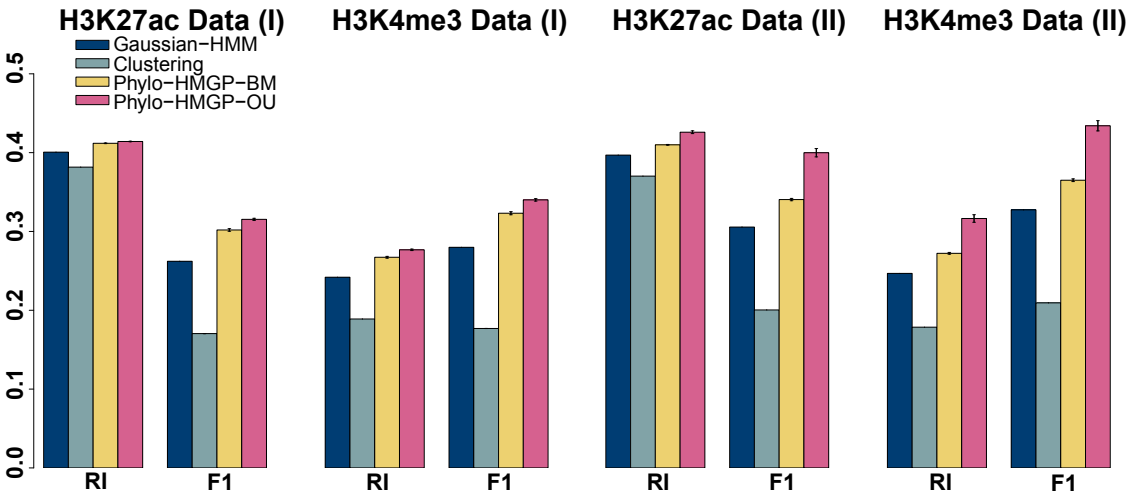

Figure S9: Evaluation of Gaussian-HMM, K-means Clustering, Phylo-HMGP-BM, and Phylo-HMGP-OU on H3K27ac and H3K4me3 ChIP-seq datasets in terms of RI (Rand Index), and F_1 score. Related to Figure 1. Experiments (I) represent they are perforemd for the four mammal species. Experiments (II) represent they are performed for the three primate species human, macaque, and marmoset. The standard error of the results of 10 repeated runs for each method is shown as the error bar.